TECHNICAL NOTE

Development of functionally gradient Cu-Fe based sintered brake pad materials

Physica Scripta

TECHNICAL NOTE

Development of functionally gradient Cu-Fe based sintered brake pad materials

RECEIVED
7 March 2024

REVISED
17 April 2024

ACCEPTED FOR PUBLICATION
3 May 2024

PUBLISHED
20 May 2024

Rajesh Kannan Kasi[1], **Nithin Kumaar Murugesan**[2], **Aishwarya Jeyakanapathy**[2], **Vaira Vignesh Ramalingam**[1,*] **and Govindaraju Myilsamy**[1]

[1] Department of Mechanical Engineering, Amrita School of Engineering, Coimbatore, Amrita Vishwa Vidyapeetham, India
[2] School of Materials Science & Engineering, University of New South Wales, Sydney, New South Wales, Australia
[*] Author to whom any correspondence should be addressed.

E-mail: r_vairavignesh@cb.amrita.edu, r.vairavignesh@gmail.com and m_govindaraju@cb.amrita.edu

Keywords: renewable energy, wind turbines, brake pads, functionally gradient, homogeneous distribution

Abstract

The world is seeking a sustainable co-existence with nature to preserve the balance of our ecosystem. This has opened a wider market for green and renewable forms of energy to realize the energy requirements of global countries. Among the various renewable energy sources, harnessing the kinetic energy of the wind through a turbine to generate electricity has seen an ardent growth. Wind turbines, in general, function between 2 m s^{-1} and 25 m s^{-1} wind speed. When the winds cross the cut-out speed (25 m s^{-1}) or during the maintenance of wind turbine components, the brakes are implemented. The primary aerodynamic and secondary mechanical brakes comprise the wind turbine braking system. The mechanical brake pads are fixed to the brake caliper. On braking, the brake caliper pushes the brake pads against the brake disc. This recurring action gradually wears the brake material. The presence of ceramic particles in the traditionally used bulk composite pads imparts poor joint properties between the brake pad and caliper. These mandate frequent replacement of the brake pads. The current research work developed a functionally gradient brake pad through the powder metallurgy technique. The microstructure, microhardness, and tribological properties of the fabricated brake pads are tested and analyzed. Microstructural analysis revealed a homogeneous distribution of the reinforcements in the metal matrix. COF was observed to be within the desired range of between 0.3 and 0.4. The brake pad exhibited a combination of adhesive-abrasive-oxidative wear.

Introduction

Energy consumption is increasing at a tremendous pace across the globe. It is determined that the energy requirement is to be increased two-fold by the middle of this century [1–3]. Based on the current trend of energy consumption, non-renewable energy resources are being used extensively when compared to renewable energy resources [4]. This trend leads to the rapid depletion of the sources and creates an energy crisis. Non-eco-friendly fossil fuels are also attributed to environmental pollution [5, 6]. This calls for the need for renewable energy resources (RER). There are different kinds of RER namely wind, water, geothermal, solar, and biomass [7]. Due to the large number of positive effects of RER, all the counties are planning to implement them at a faster pace. This would not only save resources for future generations but also have an eco-friendly sustainable development [8].

Wind energy is a renewable source that is increasing at an exponential pace. The capacity of energy generated by wind is at exponential growth [9]. Around 650 GW of energy is released from wind per year as of 2018. It is predicted that one-third of the world's electricity needs will be satisfied by wind energy by 2050. Thus, the need to establish more equipment to generate wind energy is in demand [10]. Wind turbines are installed in suitable regions to channel the energy obtained from the winds. In collaboration with the Ministry of New and

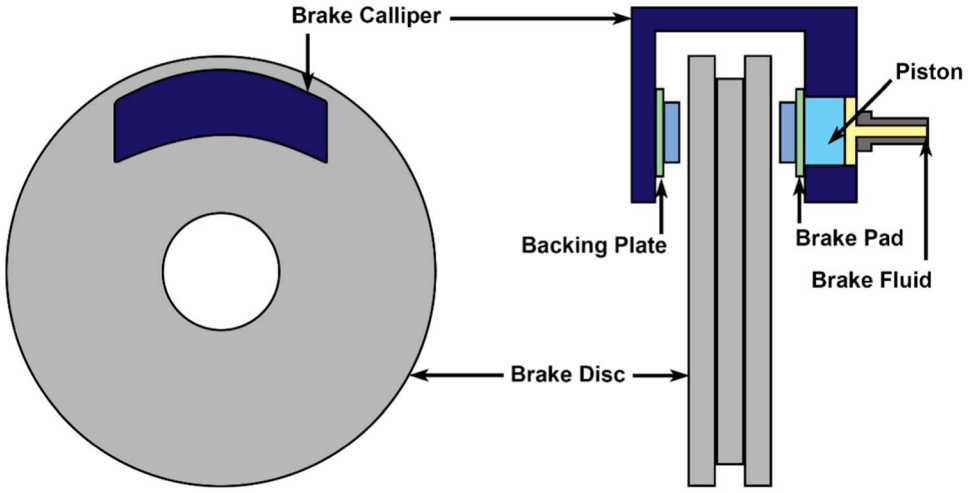

Figure 1. Schematic of a mechanical braking system.

Renewable Energy (MNRE), the Indian government plans to increase wind power generation to 60 GW by 2022. The long coastal line of India helps to harness the maximum amount of wind energy [7, 9].

Wind energy is obtained from the kinetic energy present in the wind due to its flow. This kinetic energy is used by wind turbines to generate electricity. The wind turbine has different systems which all combine to generate electricity. A conventional wind turbine has a transmission system, electrical system, support system, braking system, etc [11]. Usually, a wind turbine of 750-kW capacity operates at the nominal speed of the low-speed shaft at 18 rpm and the high-speed shaft at 1500 rpm. The wind turbine produces electricity when it runs between 2 m s^{-1} and 15 m s^{-1}. Once, the speed exceeds 10% more than the nominal speed of the lower-speed shaft, the braking system starts to work [10, 12]. First, the aerodynamic braking starts to operate. In aerodynamic braking, the blades of the wind turbine are oriented parallel to the wind flow direction. Since there is no force acting on the wind turbine blades, it starts to decelerate and reduce the speed of the lower-speed shaft. Then, the speed of the higher-speed shaft also reduces from 1500 rpm to 350–450 rpm. Once, this speed is reached by the higher-speed shaft, the mechanical brakes are applied. The schematic of the mechanical braking system in a wind turbine is depicted in figure 1. Due to the friction between the surfaces, the brake disc starts to decelerate. There is the liberation of heat energy due to the frictional energy that is generated. The wind turbine and generator stop rotating as the speed of the rotor disc is reduced by the frictional resistance between the brake pad and the disc [13].

Two major problems occur in bulk composite brake pads, commonly. Firstly, due to the poor joint strength between the brake pad and brake caliper due to the existence of hard ceramic phases (reinforcement) [14, 15]. Secondly, poor wear resistance of the brake pad between the brake pad and brake disc [16–18]. This necessitates a need for the development of new brake pad material. Functionally gradient material can be used for the brake pad.

Studies by Govindaraju *et al* [19] showed that the wear rate of functionally gradient brake pads was 98% lower than conventional brake material. Kwabena Gyimah *et al* [20] revealed that the material properties of the brake pad improved with increasing sintering temperature. Investigations by Zhang *et al* [21] showed that Cu and Fe present in the brake pad stabilized the friction coefficient and wear rate. Analysis by Xiao *et al* [22] on high-performance applications shows that Cu MMC brake materials can be used to remove spallation and dislocation of brake pads. Ma *et al* [23] compared the braking behavior of iron and copper-based brake pads used for C/C—SiC disc. The wear mechanism of the Fe-based brake pad was mainly abrasion, while the Cu-based brake pad relied on adhesion. Cu-based brake pads performed well when compared to iron brake pads [24]. Chen *et al* [25] investigated the tribological behavior of the h-BN-modified Cu metal matrix and observed that the h-BN is better suited for Cu-MMC brake pads for high-speed applications. Uyyuru *et al* [26] studied that sliding speed proportionally influences the tribolayer thickness. Research by Peng *et al* [27] on the influence of the Cu/Fe ratio and found that with an increase in Fe content stable tribo-oxides layers were formed which retards its destruction. Cu-based composites with 14 wt%Fe improved the hardness from 9.21 to 20.39HBW [28]. The friction coefficient had a substantial enhancement of 16.8% to 0.39 with the inclusion of Fe [29]. Also, Zhang *et al* [30] inferred from their studies that the plasticity of Cu provides stability to the tribolayer. Similar observations were reported by researchers [31, 32].

Table 1. Chemical composition of FG brake pad layers in wt%.

SI.	Layer	Composition
1	Layer 1	Cu-10Fe-5hBN-3SiC-2Al_2O_3
2	Layer 2	Cu-10Fe-3hBN-2SiC-2Al_2O_3
3	Layer 3	Cu-10Fe-3hBN-1SiC-1Al_2O_3
4	Layer 4	Cu

Xiao *et al* [33] tested a Cu-based brake pad for a wear mechanism developed for high-speed applications. It was observed that the worn surface was covered by a tribolayer, which consists of CuO and Fe_2O_3 nanoparticles. It can be inferred that the tribological properties of the brake pads highly depend on the composition and microstructure. Zhang *et al* [34] studied the influence of adding Al_2O_3 fiber to Cu-based brake pads used for high-speed applications. It can be inferred that Al_2O_3 fiber reinforcement reduced the wear rate and exhibited low temperature during braking.

A literature survey convinces that conventionally used bulk composite brake pads, though processed through the P/M technique, have certain utility and maintenance limitations. The reinforcements present at the interface of the brake pad and calipers reduce the joint strength. This can dislocate the brake pad from the brake calipers thereby reducing their service life. It may result in a catastrophic event if the turbine loses its control. Though many studies on Cu-Fe-based brake pads have been reported, studies on functionally gradient Cu-Fe-based brake pads are seldom discussed in the open literature. In this study, a brake pad with a functionally gradient composition was fabricated through powder metallurgy processes. The microstructure and microhardness of the brake pad were analyzed. Tribological characterization was performed to investigate wear and friction properties.

Materials and methodology

Materials

In this study, a functionally gradient brake pad was developed for wind turbine applications through the P/M technique. A typical P/M processed brake pad consists of metal matrix components, friction materials, and solid lubricants. Suitable constituent powders were chosen to render specified properties to the brake pad. In this study, Cu and Fe with a particle size of 75 μm, hBN with a particle size of 10 μm, and SiC and Al_2O_3 with a particle size of 20 μm were chosen as the base materials. Copper (Cu) stabilizes COF by introducing a film of CuO at the interface. Fe enhances the wear resistance and good braking performance at high-temperature working conditions. They also induce strength in the brake pads. h-BN, due to its superior properties, is used as a lubricating agent compared to other lubricating agents. Their unique properties include high initial oxidation temperature (900 °C), chemical stability, and to ability to perform better under elevated temperatures. Al_2O_3 and SiC are used as frictional additives. The elemental powder composition of the metal matrix (Cu, Fe) and the reinforcements (SiC, Al_2O_3, h-BN) in each layer are listed in table 1. The composition of the brake pad was framed in terms of weight percentage.

Powder metallurgy processing

Powder metallurgy processing includes blending, compaction, and sintering of the powders. The elemental powders of Cu, Fe, SiC, Al_2O_3, and h-BN were taken according to the composition, and the required powders were weighed accurately using a digital balance that has a readability of 0.0001 g. The powders were then blended using a ball milling machine to get a thorough mixture. The ball milling process was carried out using 8 mm steel balls at 250 rpm for an hour. Polyvinyl alcohol was used as a binding agent to provide structural integrity to the powders and to ensure proper bonding between the different powders. The powder mixture was cold compacted using a die and press arrangement. A uniaxial hydraulic power press with a suitable load of 0.75 tons was used for compaction. Sintering is a diffusion-assisted process where consolidation of the green product takes place. The compacted specimens wrapped with glass wool, to prevent reaction with evolved gases, were placed inside a small ceramic holder. This setup was placed inside a vacuum furnace and sintered at 950 °C for 60 min at a pressure of 10^{-3} mbar. Table 2 gives the vacuum furnace specifications used to fabricate the brake pads.

Microstructure

The fabricated brake pads were cut along the transverse direction to make a flat surface to analyze the microstructure. The specimens were prepared according to the ASTM E3-11 standards. The specimens were polished using standard metallographic sheets of different grits using an automatic disc polisher. The

Table 2. Specifications of vacuum furnace.

SI.	Contents	Specification
1	Hot Zone Effective Size	Φ50 mm × 100 mm
2	Maximum Operating Temperature	1150 °C
3	Maximum Operating Vacuum	5×10^{-5}
4	Heating Rate	10 °C/min
5	Heating Elements	Mb
6	Maximum charge weight	2 kg
7	Power Supply	6 KW
8	Operation	Thyristor controlled, PID Programmable

microstructure of the specimen was analyzed using an inverted metallurgical Optical microscope (Make: Carl Zeiss; Model: Axiovert 25).

Microhardness

The test samples for measuring microhardness were prepared as per the ASTM E3-11 standards. Vicker's microhardness test was done on the brake pad samples using a microhardness tester (Make: Mitutoyo; Model: HVT–M1), along the transverse direction. The test was carried out according to ASTM E92-17 standards. An average of five readings were taken using a diamond indenter with an axial load of 25 grams on the specimens for 15 seconds as dwell time.

Tribological characterization

The tribological test specimens were secured to a hollow steel tube using an M-seal for support. The test specimens were polished, cleaned using acetone, and weighed on a precision scale before testing. The wear tests were carried out according to ASTM G99-5a standards in a pin-on-disc tribometer (Make: Ducom; Model: TR-2OLE-PHM-200). The specimen was securely affixed to a collet and positioned against the counter disc made of EN31 steel. Normal loads of 5 kg and 7 kg were applied at the contact point using a lever mechanism. The specimens were slid at a sliding velocity of 5.5 m s^{-1} at each normal load in triplicates for wear evaluation. The specimens were weighed again after testing to obtain the mass loss to calculate the wear rate. The frictional force acting between the specimen and the counter disc is obtained from the friction force monitor. The coefficient of friction of the test sample is obtained by using the friction force and normal force acting on it [35, 36].

The justification for the wear test parameters are as follows: The brake pad is designed for a wind turbine of 750 kW capacity. The nominal speed of the low-speed shaft of the turbine is 18 rpm and that of the high-speed shaft is 1500 rpm. The brake is designed to operate at 10% over the speed of the low-speed shaft. The design calculations are given by equations (1) to (4).

$$P = T \times \omega \tag{1}$$

$$\Rightarrow T = P/\omega \tag{2}$$

$$\Rightarrow T = \frac{P \times 60}{2 \times \pi \times N} \tag{3}$$

$$\because \omega = \frac{2 \times \pi \times N}{60} \tag{4}$$

At 1500 rpm, the developed torque in the high-speed shaft is 9554.14 Nm. The shaft diameter should be 110 mm to sustain the torque, as per the design guidelines of PN-M-85 000: 1998. A 10% increase in low-speed shaft with 1.1 factor for possible loss of caliper spring force results in 22 rpm, and correspondingly high-speed shaft results in 1650 rpm. Hence, the angular velocity of the high-speed shaft is 172.7 m s^{-1}.

Considering the super-critical sliding velocity as 40 m s^{-1}, the brake disc diameter is found to be 0.46 m. The power dissipation at the instance of braking is 1649.28 kW, which is calculated by the equation (5).

$$Q_b = T \times \omega \tag{5}$$

The thermal design constraint for brake pads is that the maximum power dissipation per unit pad area (Q) should be below 11.6 MW m^{-2}. Hence, the total area of pads is given by the ratio of Q_b and Q. The total area of pads is 0.142 m^2, which would be covered by 4 calipers fitted with brake pads of 0.17 m × 0.17 m. When the turbine reaches over-speed, the high-speed shaft is decelerated to rotations less than 450 rpm by an aerodynamic brake. Then, the mechanical brakes are applied on the high-speed shaft between 350 rpm and 450 rpm. Based on

the above design considerations, the sliding velocity at 55 mm from the axis is 2.0 m s^{-1} and 142.5 mm from the axis (brake pad position) is 5.2 m s^{-1}. Hence, the sliding velocity for the wear test was fixed as 5.5 m s^{-1}. The axial load of 5 kg (∼50 N) and 7 kg (∼70 N) simulate the actual contact stress conditions, when the brake pads are pressed against the brake disc using a hydraulic setup. Also, the brake pads are actuated momentarily to avoid the fading effect.

Characterization using analytical instruments

The surface characteristics of the worn-out samples were observed using a Field Emission Scanning Electron Microscope (FE-SEM). Surface morphology was scrutinized at various magnifications at appropriate acceleration voltage. The elemental composition of the specimens was obtained through EDS analysis. x-ray diffraction (Make: Rigaku; Model: Ultima 4). was done to study the various phases present in the matrix. The graphs were attained corresponding to Cu- Kα radiation at a scan rate of 0.5° per minute in continuous scanning mode.

Results and discussions

Microstructure

The microstructure of the fabricated functionally gradient brake pad, as shown in figure 2, exhibited distinct characteristics. Detailed information about the composition of the various gradient layers can be found in table 1. Starting from the bottom-most layer, it consisted solely of pure elemental Cu. The deliberate choice of using pure elemental Cu in this layer was to enhance the bonding properties between the brake pad and the brake caliper. The presence of Cu facilitated the formation of a robust metallic bond at the interface, ensuring a secure joint. The concentration of reinforcements varied as one traversed across the volume of the pad. Gradually, from the bottom to the top layers, the concentration of reinforcement particles increased. At the uppermost layer, the maximum concentration of these reinforcements was observed [37].

The primary purpose of such distribution of reinforcement particles was to enhance the wear resistance between the brake pad and the brake disc. By incorporating the particles, the brake pad's ability to withstand frictional forces and maintain its integrity during prolonged use was significantly improved. Also, a uniform distribution of reinforcements throughout the different layers was observed. The uniform dispersion ensured that the benefits of the reinforcements were effectively utilized across the entire volume of the brake pad. Such uniformity in reinforcement distribution is essential to maintain consistent performance and prevent localized wear or stress concentrations. The meticulous material selection and dispersion, combined with a well-executed sintering cycle resulted in the absence of any cracks in the microstructure of the sintered specimen. The absence of cracks indicated that the pad would be less prone to failure and would have enhanced reliability during braking operations. Figure 6 (Cu-FGM) clearly illustrates the phase analysis of the sintered specimens. The results inferred that the elements incorporated are present in their innate forms. There was no evidence of any reactions between the constituents present in the system.

Microhardness

The Vicker's microhardness values indicate the resistance to indentation and deformation. The testing was conducted along the cross-section of the pad, allowing for an assessment of the hardness distribution across different layers. In figure 3, the graph displays the average microhardness values obtained from the measurements. The first gradient layer showed the highest average microhardness value of 173.8 HV, indicating its superior hardness compared to the other layers. The high hardness was attributed to the presence of a higher concentration of reinforcement particles within this layer. At the interface between the first and second gradient layers, the average microhardness decreased to 121.3 HV. The reduction in microhardness suggested the transition from a highly reinforced region to a relatively less reinforced one. The microhardness of the second gradient layer was measured to be 104.5 HV, indicating a lower concentration of reinforcement particles compared to the first layer.

The interface between the second and third gradient layers exhibited a microhardness of 76.2 HV, indicating a further decrease in hardness. The third gradient layer displayed a mean microhardness of 51.4 HV, indicating a relatively lower concentration of reinforcement particles compared to the preceding layers. At the interface between the third and fourth gradient layers, the microhardness decreased to 34.2 HV. Finally, the last layer, which consisted of pure Cu without any reinforcement elements, recorded the lowest hardness value of 19.4 HV. The observed trend in microhardness values suggests that the presence and concentration of hard reinforcement particles linearly influence the microhardness of each layer. As the concentration of ceramic particles increased through the layers, the microhardness values also increased accordingly. The homogeneous distribution of reinforcement particles within each layer further contributed to the rise in hardness values. Moreover, the

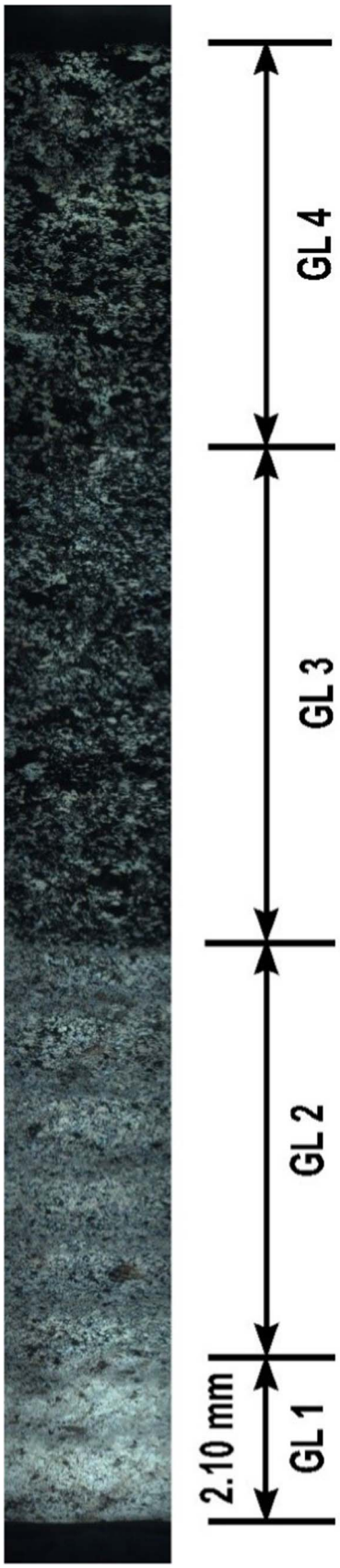

Figure 2. Microstructure of the fabricated sintered FGM brake pad.

sintering temperature played a role in determining the density of the brake pads. Higher sintering temperatures resulted in denser brake pads, which, in turn, improved their hardness values. This densification process enhanced the wear-resistant properties of the brake pad, as wear properties tend to improve with hardness.

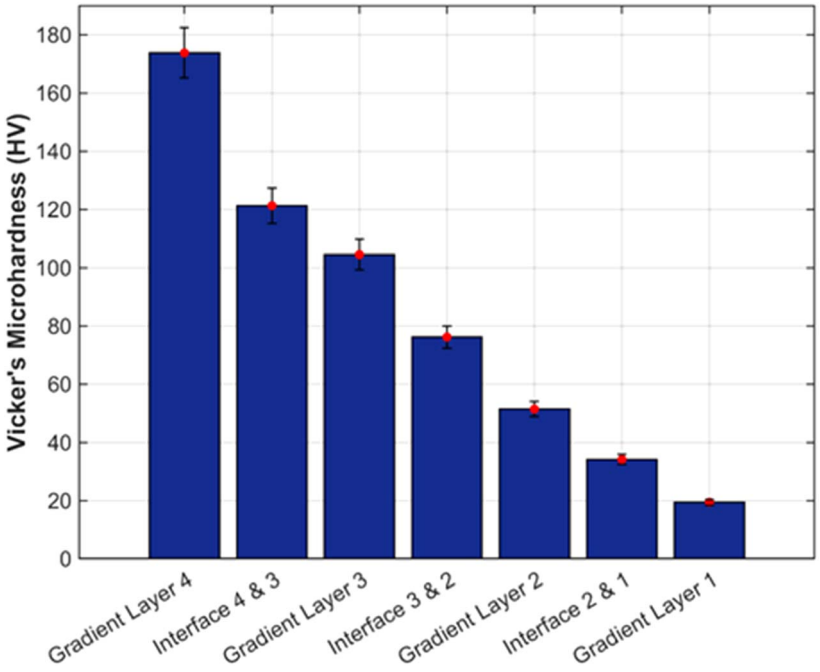

Figure 3. Microhardness of the brake pad along with the layers.

Table 3. Mass loss and wear rate at different loading conditions.

Load(kg)	Mass loss (g)	Wear rate (g/Nm)
5	0.0289	3.3077×10^{-7}
7	0.0670	5.4774×10^{-7}

Tribological characterization

The tribological characteristics of the brake pad were evaluated using a pin-on-disc tribometer, The tribometer was operated at a sliding velocity of 5.5 m s^{-1}, and different loads of 5 kg and 7 kg were applied for 10 min. The wear rate of the brake pad was measured against the various loads. The wear rate increased as the load applied to the brake pad increased from 5 kg to 7 kg. This finding suggests that higher loads exerted greater stress on the interface between the brake pad and the counter disc, resulting in increased wear. Table 3 provides detailed information on the mass loss and wear rate sustained by the brake pad under different loads [38].

As the load on the brake pad increased, the friction at the interface between the pad and the counter disc also increased. This heightened frictional force caused more material to be worn away from the surface of the brake pad, leading to a greater mass loss and higher wear rate. The friction generated during the sliding contact not only influenced the wear rate but also had an impact on the temperature at the contact region between the brake pad and the counter disc. The increase in friction resulted in higher temperatures, as the energy dissipated as heat due to the frictional forces. This rise in temperature at the contact interface could have additional effects on the tribological behavior of the brake pad, such as changes in the coefficient of friction and the formation of frictional hotspots.

The coefficient of friction (COF) of the fabricated functionally gradient (FG) brake pads was determined using a pin-on-disc tribometer under various loading conditions. For the specific loading conditions of 5 kg and 7 kg, the COF values were measured to be 0.3744 and 0.3920, respectively. The COF increased as the load applied to the brake pads increased from 5 kg to 7 kg. However, the changes in COF values were not drastic with the addition of loads. This suggests that the COF response of the brake pads was relatively stable and less influenced by variations in the applied load. The increase in COF with increasing load can be attributed to the flattening of the hard particle asperities present at the contact region between the brake pad and the counter disc. As the load increased, the pressure exerted on the brake pad also increased, causing the asperities to deform and create more contact area, thus leading to an increase in the COF value. The COF range considered desirable for optimum performance of wind turbine brake pads is typically between 0.3 and 0.4. The experimentally determined COF

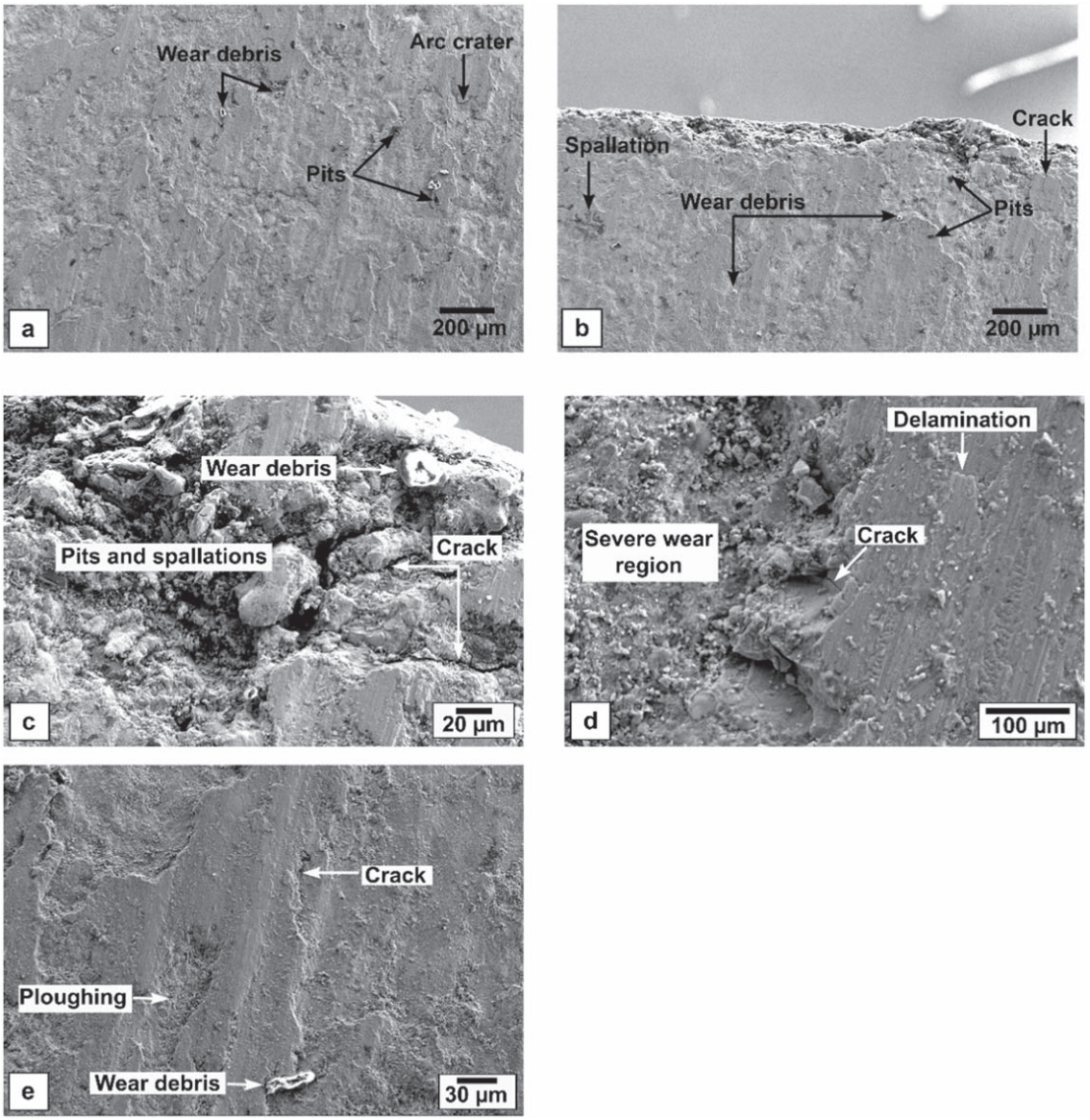

Figure 4. Characteristic wear surface of the brake pad under 5 kg loading conditions.

values for the FG brake pads fell within the desired range. This indicates that the brake pads exhibited favorable COF characteristics, which is crucial for efficient braking performance in wind turbine applications.

Wear mechanism

Figures 4 and 5 show the worn surface characteristics of the specimen, showcasing the effects of different loading conditions: 5 kg and 7 kg, respectively. When a normal load of 5 kg was applied to the brake pad, the worn surface exhibited distinct features such as minuscule pits and arc craters shown in figure 4(a). The surface irregularities were indicative of the adhesive-wear process that occurred during tribological experimentation. The metallic particles were gradually removed from the contact region, eventually settling as debris on the worn surface shown in figures 4(a)–(c), and (e). In addition, a few ceramic particles were forcefully expelled from the pad surface during the braking process, resulting in a phenomenon known as spallation represented in figure 4(b). Notably, figure 4(e) provides a visual representation of the plowing effect that was observed. Moreover, cracks were observed in figures 4(b) and (e) in certain regions of the fractured specimen, serving as evidence of severe deformation.

Under a normal load of 7 kg, the worn-out surface of the brake pad displayed delamination characterized by the separation of layers parallel to the surface illustrated in figure 5(a). The delamination was a consequence of the cyclic impact experienced during tribological testing. Upon closer examination, continuous scratches in figure 5(c) and shallow furrows in figure 5(d) were observed on the wear surface, indicating the occurrence of scoring and localized scuffing. The surface irregularities and cracks shown in figure 5(b) were formed due to the

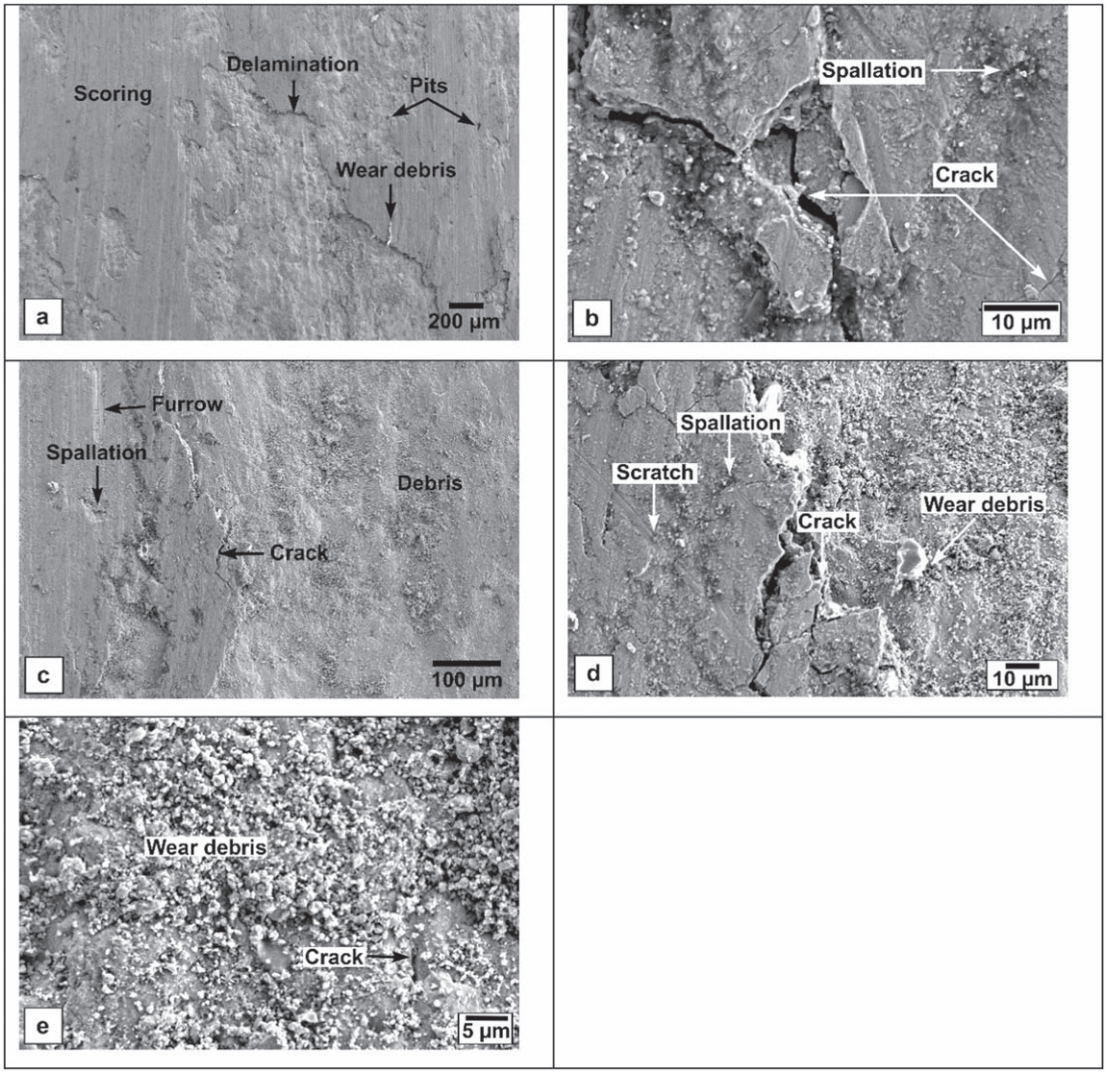

Figure 5. Characteristic wear surface of the brake pad under 7 kg loading conditions.

trailing of hard particles across the brake pad surface. The wear debris was scattered on the worn surface presented in figures 5(d) and (e). The worn surface revealed complex wear characteristics, including severe abrasive wear along with mild adhesive wear.

Furthermore, energy-dispersive x-ray spectroscopy (EDS) analysis was performed to examine the elemental composition at various regions of the brake pads. Figure 7 (a)–(c) illustrates the results obtained from the wear-tested specimen. The EDS analysis revealed a high concentration of oxygen in the wear surface. Remarkably, the amount of oxygen detected in the worn surface was nearly equivalent to the amount of copper (Cu) present in the base matrix of the brake pad. This finding strongly indicates the formation of metal oxides during the braking process, further corroborating the oxidative wear mechanism at play. Thus, it can be concluded that a combined adhesive-abrasive-oxidative wear mechanism occurred in this brake pad under conventional braking conditions, as supported by the surface characteristics, fractographs, XRD analysis, and EDS results.

The composition of the brake pad, wear debris, and worn surface was analyzed using XRD. The XRD pattern revealed distinctive peaks that corresponded to both copper (Cu) and iron (Fe), confirming their presence in the composition of the brake pad. Moreover, significant peaks corresponding to the reinforcements Al_2O_3, SiC, and h-BN were visualized, indicating their contribution to the composition and properties of the brake pad. Figure 6 provides an overview of the different phases and constituents identified in the brake pad after the wear test, providing a comprehensive understanding of its composition and potential wear mechanisms.

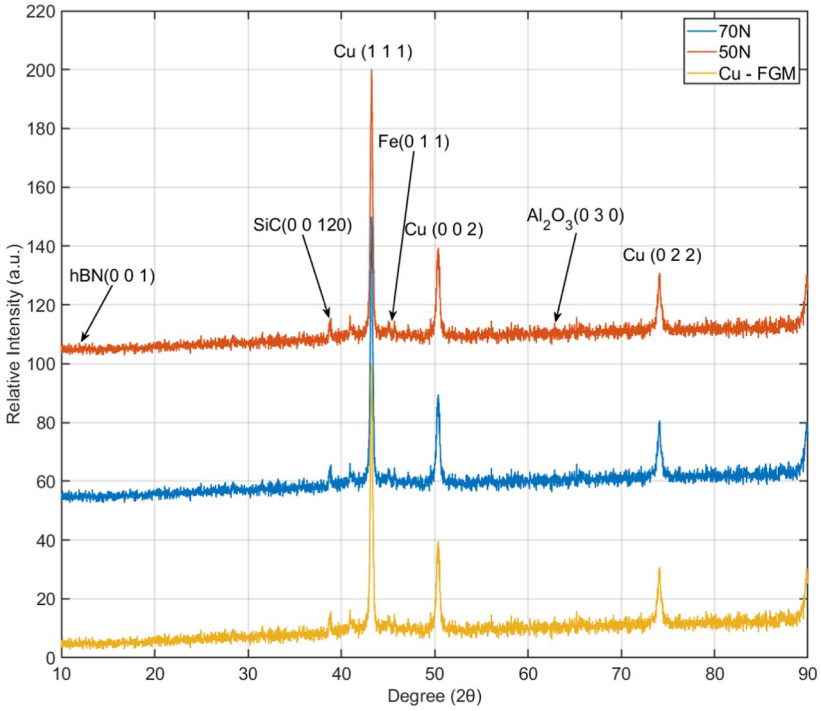

Figure 6. XRD graphs of the worn brake pads.

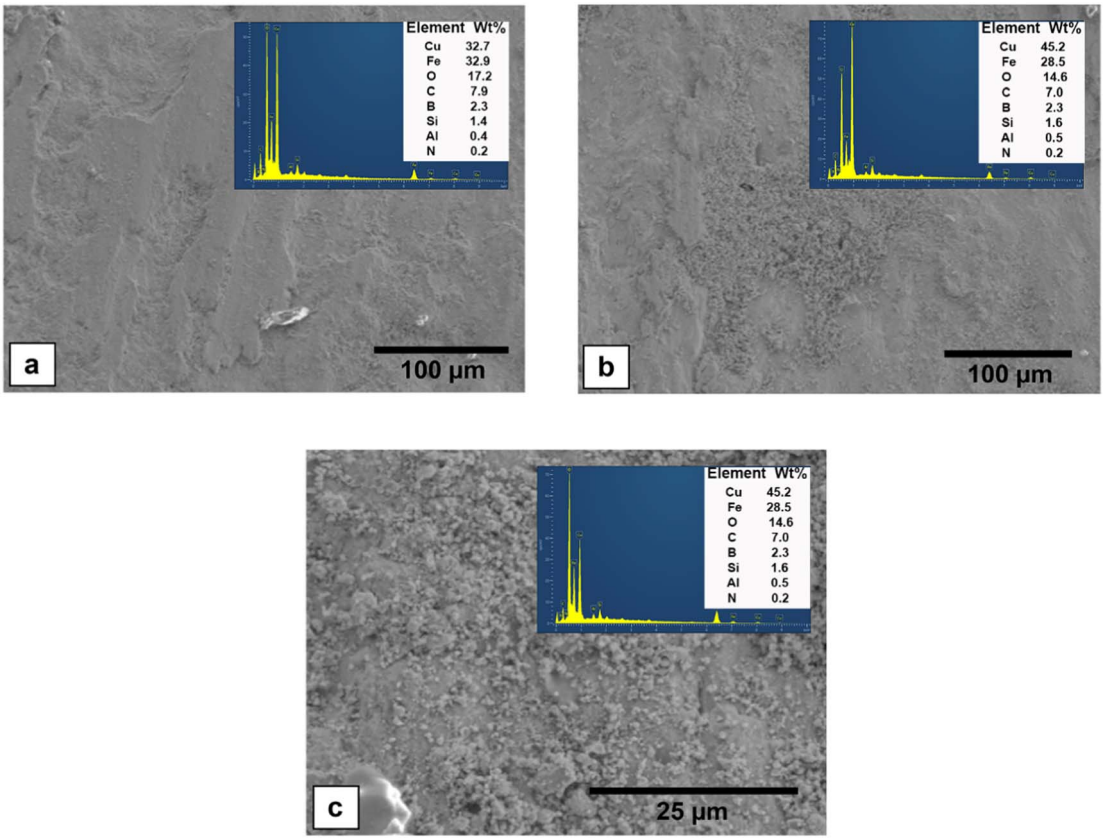

Figure 7. Elemental composition of the brake pads.

Conclusions

The powder metallurgy processing technique was successfully applied to fabricate a functionally gradient Cu-Fe based sintered brake pad materials. The microstructure, microhardness, wear rate, coefficient of friction, and wear mechanism of the fabricated specimens were analyzed. The results demonstrated the following:

- The microstructural analysis shows that the reinforcement particles are distributed homogeneously through the layers. The absence of reinforcements at the interface of the brake pad and brake caliper enhances the joint strength. The presence of a large number of reinforcement particles at the contact region (brake pad-brake disc) gives better wear resistance properties to the brake pads.
- Microhardness measurement shows a continuous increase in values with increased reinforcement concentration. The topmost gradient layer exhibits a maximum value of 173.8 HV while the first layer with pure Cu had a hardness value of 19.4 HV.
- As the load acting on the brake pad increases, the wear rate and COF of the specimens increase. The wear rate increased from 3.3077×10^{-7}g/Nm for 5 kg to 5.4774×10^{-7} g/Nm for 7 kg axial load. The COF values increased from 0.3744 for 5 kg to 0.3920 for 7 kg load. The obtained COF values were in the desired range of 0.3 to 0.4.
- The wear surface morphology depicted that a combination of adhesive-abrasive-oxidative wear had occurred.

Data availability statement

All data that support the findings of this study are included within the article (and any supplementary files).

Declarations

Funding

The authors are obligated to the Department of Science and Technology and Quantum Heat Treaters Pvt. Ltd Coimbatore for their financial support to carry out the research work. The authors are grateful to perform the investigation under the research title 'Development, Field Trials, Pilot Production, and Technology Demonstration of Sintered Brake Pads with Improved Performance for Wind Turbine Applications Suitable to India Specific Wind Characteristics' (DST/TDT/AMT/2017/002(G)).

Conflicts of interests

The authors declare that there is no conflict of interest or competing interests for the research work.

Data availability

All data generated or analyzed during this study are included in this published article.

Code availability

Not Applicable

Ethics approval

Not Applicable

Consent to participate

Not Applicable

Consent for publication

Not Applicable

Author contributions

Rajesh Kannan Kasi, Formal analysis, **Nithin Kumaar Murugesan**, Investigation, Software, Visualization, Writing - Original Draft, **Aishwarya Jeyakanapathy**, Investigation, Software, Writing - Original Draft, **Dr Vaira Vignesh Ramalingam**, Methodology, Validation, Supervision, Writing - Review & Editing, **Dr Govindaraju Myilsamy**, Conceptualization, Resources, Funding acquisition

ORCID iDs

Vaira Vignesh Ramalingam https://orcid.org/0000-0002-6869-1763

References

[1] Agency I E (ed) 2020 *Global Energy Review* 2020 (IEA Paris)
[2] Agency I E (ed) 2019 *Key World Energy Statistics* 2019 (IEA Paris, France)
[3] Bogmans C, Kiyasseh L, Matsumoto A and Pescatori A 2020 Energy, efficiency gains and economic development: when will global energy demand saturate? *International Monetary Fund*
[4] Data OWi Global primary energy consumption by source [Available from: https://ourworldindata.org/grapher/global-energy-substitution?country=~OWID_WRL
[5] Agency IE INDIA [Available from: https://www.eia.gov/international/analysis/country/IND
[6] Panchasara H, Samrat N H and Islam N 2021 Greenhouse gas emissions trends and mitigation measures in australian agriculture sector—a review *Agriculture* **11** 85
[7] Roser HRaM 2020 Renewable Energy OurWorldInData.org[Available from: https://ourworldindata.org/renewable-energy
[8] Yang P 2024 *Wind Power. Renewable Energy: Challenges and Solutions* (Springer) 73–107
[9] VANADIUMCORP 2016 Vanadium redox flow batteries: the next big wave after lithium batteries [Available fromhttps://www.vanadiumcorp.com/news/industry/vanadium-redox-flow-batteries-the-next-big-wave-after-lithium-batteries/?hcb=1
[10] Ranjan R 2020 *2.07 GW of Wind Power Capacity Installed in India During FY 2019-20* (Mercom Capital Group, LLC) [Available from: https://mercomindia.com/2-07-wind-power-capacity-installed-india/
[11] Data OWi Wind power generation [Available from: https://ourworldindata.org/grapher/wind-generation?tab=chart
[12] Raafat S and Hussein R 2018 Power maximization and control of variable-speed wind turbine system using extremum seeking *Journal of Power and Energy Engineering* **06** 51–69
[13] Sai Balaji M, Katiyar J K, Eakambaram A, Baskara Sethupathi P, Kamalakannan J and Baskar A 2023 Comparative study of sintered and composite brake pad for wind turbine applications *Proceedings of the Institution of Mechanical Engineers, Part J: Journal of Engineering Tribology* **237** 1430–45
[14] Govindaraju M *et al* 2020 Investigations on the tribological behavior of functionally gradient iron-based brake pad material *Proc. Inst. Mech. Eng. Part C J. Mech. Eng. Sci.* **234** 2474–86
[15] Guha Keshav M, Hemchandran C G, Pradhin K, Vaira Vignesh R and Govindaraju M 2019 Manufacturing of continuous fiber reinforced sintered brake pad and friction material *Mater. Today. Proc.* **46** 4493–6
[16] Rajesh Kannan K, Govindaraju M and Vaira Vignesh R 2021 Development of fly ash based friction material for wind turbines by liquid phase sintering technology *Proc. Inst. Mech. Eng. Part J J. Eng. Tribol.* **235** 1463–9
[17] Rajesh Kannan K, Vaira Vignesh R, Pavan Kalyan K, Murugesan J, Megalingam A, Padmanaban R and Govindaraju M 2019 Tribological performance of heavy-duty functionally gradient friction material (Cu-Sn-Fe-Cg-SiC-Al2O3) synthesized by PM route *AIP Conf. Proc.* **2128** 020004
[18] Takeda S, Miki H, Takeishi H and Takagi T 2017 Cu-Based MoS2-dispersed composite material formed by the compression shearing method at room temperature *Tribology Online* **12** 29–36
[19] Govindaraju M, Megalingam A, Jayaprakash Murugasan, R Vaira Vignesh, Pavan Kalyan Kota, A Sumanth Ram, P Lakshana and V Naveen Kumar 2020 Investigations on the tribological behavior of functionally gradient iron-based brake pad material *Proc. Inst. Mech. Eng. Part C J. Mech. Eng. Sci.* **234** 2474–86
[20] Kwabena Gyimah G, Huang P and Chen D 2014 Dry sliding wear studies of copper-based powder metallurgy brake materials *J. Tribol.* **136** 041601
[21] Zhang P, Zhang L, Fu K, Cao J, Shijia C and Qu X 2018 Effects of different forms of Fe powder additives on the simulated braking performance of Cu-based friction materials for high-speed railway trains *Wear* **414** 317–26
[22] Xiao Y *et al* 2018 Mechanical and tribological behaviors of copper metal matrix composites for brake pads used in high-speed trains *Tribology International* **119** 585–92
[23] Ma X, Luan C, Fan S, Deng J, Zhang L and Cheng L 2021 Comparison of braking behaviors between iron-and copper-based powder metallurgy brake pads that used for C/C–SiC disc *Tribology International* **154** 106686
[24] Shibata K, Yamaguchi T, Mishima J and Hokkirigawa K 2008 Friction and wear properties of Copper/Carbon/RB ceramics composite materials under dry condition *Tribology Online* **3** 222–7

[25] Chen F et al 2021 Tribological behavior and mechanism of h-BN modified copper metal matrix composites paired with C/C–SiC Tribol. Int. 153 106561
[26] Uyyuru R, Surappa M and Brusethaug S 2007 Tribological behavior of Al–Si–SiCp composites/automobile brake pad system under dry sliding conditions Tribol. Int. 40 365–73
[27] Peng T, Yan Q, Zhang X and Zhuang Y 2020 Role of titanium carbide and alumina on the friction increment for Cu-based metallic brake pads under different initial braking speeds Friction 9 1543–57
[28] Zheng D et al 2023 Effects of Fe and graphite on friction and wear properties of brake friction materials for high-speed and heavy-duty vehicles Tribology International 178 108061
[29] Wu S et al 2023 Effect of Iron powder type on friction and wear properties of copper-based friction powder metallurgy material Tribology Transactions 66 1019–25
[30] Zhang P et al 2020 A high-performance copper-based brake pad for high-speed railway trains and its surface substance evolution and wear mechanism at high temperature Wear 444 203182
[31] Sato T, Hirai Y, Fukui T and Usami H 2016 Tribological properties of bronze containing micro sized sulfide -application of atomic force microscopy Tribology Online 11 195–202
[32] Alkelae F and Sasaki S 2020 Tribological and mechanical characterization of nickel aluminium bronze (NAB) manufactured by laser powder-bed fusion (L-PBF) Tribology Online 15 126–35
[33] Xiao J-K, Xiao S-X, Chen J and Zhang C 2020 Wear mechanism of Cu-based brake pad for high-speed train braking at speed of 380 km/h Tribology International 150 106357
[34] Zhang P et al 2019 The effect of $Al2O_3$ fiber additive on braking performance of copper-based brake pads utilized in high-speed railway train Tribology International 135 444–56
[35] Kannan K R, Vignesh R V, Govindaraju M and Kumar P S R 2024 Influence of rare earth oxide and graphite on the mechanical and tribological properties of Fe/Cu based sintered friction materials Science of Sintering 56
[36] Cristescu A C and Filip I 2024 Structural and tribological analysis of braking system materials disc with brake pads Appl. Sci. 14 3523
[37] Chen Q, Shang J and Xue E 2024 Tribological behavior and wear mechanism of Cu-SiO_2 sintered composite under different sliding speeds Crystals 14 232
[38] Elkady O 2024 Studying the effect of different lubricant materials on the tribological properties & hardness of Cu-Fe composite prepared By PM J. Mate. Poly. Sci. 4 1–5 https://unisciencepub.com/abstract/studying-the-effect-of-different-lubricant-materials-on-the-tribological-properties-hardness-of-cu-fe-composite-prepared-by-pm/